

A Unified Baseline Grid about the Common Research Model Wing-Body for the Fifth AIAA CFD Drag Prediction Workshop

John C. Vassberg*

Boeing Research & Technology, The Boeing Company, Huntington Beach, CA 92647

Abstract

This paper presents a unified baseline grid family under development for the Fifth AIAA CFD Drag Prediction Workshop. Foundation of the unified system is a family of point-matched multi-block grids. This sequence of grids is built from an *extra-fine* multi-block mesh about the NASA Common Research Model Wing-Body configuration. A *super-fine* mesh is then created by increasing the number of cells in each computational direction by a factor of 1.5, while maintaining grid distribution. The ratio of hexahedral cells between the extra-fine and super-fine meshes is $3.375 = 1.5^3$. These two mesh systems correspond to grid levels 5 & 6, respectively, of the multi-block grid family. To complete the even set of grid levels [2, 4, 6], the super-fine grid is recursively coarsened, consistent with the multigrid technique. In a similar manner, the odd set, comprised of grid levels [1, 3, 5], is constructed beginning with the extra-fine grid. These two groups are then interleaved to yield the final multi-block family of 6 self-consistent grids. Sizes of these grids range from 638,976 hexahedra of the *tiny* grid system, to 138,018,816 cells of the *super-fine* level, a grid-size-ratio of 216. The foundational multi-block grid family will then be converted to other grid types, such as over-set grids and unstructured meshes. Unstructured-grid systems will include families comprised of: 1) all tetrahedral elements, 2) all hexahedral cells, and 3) mixed elements of tetrahedra, prisms, and pyramids.

Nomenclature

AR	Wing Aspect Ratio = $\frac{b^2}{S_{ref}}$	S_{ref}	Reference Area
CFD	Computational Fluid Dynamics	SOB	Side-of-Body
C_{ref}	Wing Reference Chord \simeq MAC	TE	Wing Trailing Edge
DPW	Drag Prediction Workshop	WB	Wing/Body
i	Grid Index	x	Streamwise Cartesian Coordinate
j	Grid Index	X_{ref}	Moment Reference Center
k	Grid Index - Surface-Normal Direction	Y^+	Wall Distance = $Re\sqrt{\frac{c_f}{2}}y$
L	Number of Levels in Grid Family	y	Lateral Cartesian Coordinate
LE	Wing Leading Edge	z	Vertical Cartesian Coordinate
M	Number of Multigrid Levels	$3D$	Three Dimensional
MAC	Mean Aerodynamic Chord	Δ_1	Wall Spacing
n	Arbitrary Integer	λ	Wing Taper Ratio
NC	Number of Cells in One Direction	$\Lambda_{c/4}$	Wing Quarter-Chord Sweep
$RANS$	Reynolds-Averaged Navier-Stokes	∞	Signifies Freestream Conditions

*Boeing Technical Fellow, Fellow AIAA

I. Introduction

During the first decade of the 21st Century, the AIAA CFD Drag Prediction Workshop Series¹⁻⁸ (DPW) has become an invaluable resource for Computational Fluid Dynamics (CFD) and Aerodynamic Design (AD) communities worldwide. One of the charter objectives of DPW is to assess the state-of-the-art of CFD accuracy across the industry. One approach utilized in attempts to accomplish this objective has been to conduct grid-convergence studies. Corresponding results from DPW-II through DPW-IV have been somewhat mixed in this regard. Although other factors as turbulence models and stencil types play a role in the accuracy of CFD simulation, it has been generally accepted that the quality of the mesh is of paramount importance. In previous workshops, the baseline grids of the different grid classes have been inconsistently developed. Gridding Guidelines have been used to help minimize grid differences, however, this has only worked so well. As a consequence, DPW-V will include a grid-convergence test-case which is based on a unified grid system about the wing-body configuration of the NASA Common Research Model (CRM).

This paper is organized in the following manner. Section II provides a description of the baseline wing-body CRM geometry. Section III discusses the significance of selecting appropriate dimensions for the grid family. Section IV introduces a template mesh that is used to help develop the grid topology of the unified system. Section V describes the foundational multi-block grid system under construction for DPW-V. Section VI summarizes the work presented herein. Tables of data are embedded within the text, while all figures are appended to the end of the paper.

II. CRM Geometry Description

The baseline wing-body (WB) configuration for DPW-V is that of the NASA Common Research Model (CRM). Isometric views of the CRM WB configuration are shown in Figures 1-2. The CRM is representative of a contemporary transonic commercial transport designed to cruise at $M = 0.85$ and $C_L = 0.5$ at a nominal altitude of 37,000 ft. However, a couple of features have been designed into this shape solely for the purposes of research and developments. For example, the upper-surface pressure recovery over the outboard wing is intentionally made aggressively adverse over the last 10-15% local chord. The purpose for designing in this feature is to weaken the health of the upper-surface boundary layer in close proximity to the wing trailing edge (TE). This provides a fairly controlled TE separation, which is a flow phenomena under study by the DPW organizing committee. This pressure architecture also amplifies the differences between the various turbulence models, *e.g.* skin-friction drag levels. Another aspect of the CRM design that is not consistent with a real airplane design is related to its spanload. The CRM wing-body spanload is closer to elliptic than typical aircraft designs. Incorporating this feature is motivated by possible future workshops on optimization. For a purely aerodynamic shape optimization, the CRM represents a challenging case in that the optimizers will not be able to extract much improvement by simply manipulating spanload distributions. However, due to the aforementioned TE pressure recovery, the aerodynamic performance of the CRM can be improved by $\sim 2\%$. This level of potential improvement is consistent with that faced by a typical drag-reduction study on an existing aircraft.

Reference quantities and other pertinent information for the CRM are provided below.

S_{ref}	594,720.0 $in^2 = 4,130 ft^2$	[458.89 m^2]	X_{ref}	1,325.9 in	[33.68 m]
S_{trap}	576,000.0 $in^2 = 4,000 ft^2$	[444.44 m^2]	Y_{ref}	468.75 in	[11.91 m]
b	2,313.5 $in = 192.8 ft$	[58.765 m]	Z_{ref}	177.95 in	[4.520 m]
C_{ref}	275.800 $in = 16.07 ft$	[4.8978 m]	$\Lambda_{C/4}$	35.0°	
AR	9.0		λ	0.275	

For the purpose of other endeavors and experimental investigations, the CRM also includes pylon-nacelles, and a horizontal tail. The nacelles are single-path, flow-through designs with an unforced mass-flow-ratio typical of a commercial transport at cruise conditions. The aft-fuselage includes a scrubbing detail that allows the horizontal-tail to articulate through incidence while maintaining a seal at the side-of-body. The CRM wing is designed to perform exceptionally well with or without the pylon-nacelle group. For more detailed information on this geometry, see Vassberg.¹⁰

The next section addresses some practical issues related to the dimensions of a structured-mesh family.

III. Grid-Family Numerology

In order to conduct a mathematically-rigorous grid-convergence study, a sequence of parametrically-similar meshes must be established. Furthermore, the grid resolutions of this sequence must extend well into the asymptotic range of convergence. Preferably, the asymptotic behavior of grid convergence should be captured with at least 3 or 4 grid levels. Unfortunately, this can lead to very large meshes, even for the simplest 3D problems of interest under study by the DPW. To help alleviate this issue, prior workshops have adopted a 2-to-3-cell grid-refinement strategy for structured grids, in favor of the 1-to-2-cell approach. In 3D, grids constructed with 2-to-3 refinement grow in size by a factor of $3.375 = 1.5^3$ from one grid level to the next. This guideline has proven successful in controlling the size of the largest meshes, while keeping the number of grid levels in a family to a reasonable count. Both of these characteristics help minimize the workload of the DPW participants. However, the 2-to-3 refinement places a constraint on the grid dimensions, which can become a burden. For example, consider a family of 4 grids, comprised of coarse (C), medium (M), fine (F), and extra-fine (X) meshes. In the context of DPW, the medium grid corresponds to the current standard practice for accurate drag predictions. Computing the flow solution on the extra-fine mesh can be very expensive. Hence, it is imperative to design an extra-fine mesh that allows several levels of multigrid to facilitate solution convergence. If 3 levels of multigrid are desired on the extra-fine mesh, then the grid cell dimensions must be $NC_X = 4 * n$, where n is an integer. Since $NC_F = \frac{2}{3}NC_X = \frac{2}{3} * 4 * n$, then n must also be an integer-multiple of 3. This requires that $NC_X = 12 * n$, where n is an integer. Recursively applying the factor of $\frac{2}{3}$ to the medium and coarse meshes ultimately yields the constraint that NC_X must be an integer-multiple of 108 in this example. In general,

$$NC_L = 3^{(L-1)} * 2^{(M-1)} * n \quad (1)$$

Here, L is the number of levels in the grid family, M is the number of multigrid levels needed in the L^{th} grid, and n is an arbitrary integer. For the example above, $L = 4$ and $M = 3$, therefore $NC_4 = 3^3 * 2^2 * n = 108 * n$. Ironically, the coarsest grid supports the most multigrid levels, while the finest grid supports the least.

In this work, an alternative approach to developing the grid family is utilized. Here, the growth in cell count from an odd-level to the next higher even-level is given by the 2-to-3 ratio, whereas the growth from an even-level to the next higher odd-level is based on a 3-to-4-cell refinement. With this 2-to-3-to-4 strategy, the 4-grid family of the above example with 3 levels of multigrid on the extra-fine mesh requires cell dimensions of $[4, 6, 8, 12] * n$ for the $[C, M, F, X]$ grid levels, respectively. In general,

$$NC_L = \begin{cases} 3 * 2^{(M-1)} * n & ; L \text{ even} \\ 2^{(M-1)} * n & ; L \text{ odd} \end{cases} \quad (2)$$

Comparing Eqns (1-2) illustrates that the 2-to-3-to-4 refinement significantly relaxes the constraint on grid dimensions. However, it yields a grid sequence whose sizes are not evenly spaced on a log scale, as shown in Figure 3, where $Log\left(\frac{\Delta X_L}{\Delta X_1}\right)$ is plotted against grid level L .

The primary advantage of the present grid family is related to computing the full set of flow solutions for the grid-convergence studies. Most structured-mesh CFD methods incorporate both grid-sequencing and multigrid in their solution-convergence process. As a consequence, all force and moment data across the grid family can be generated with just 2 flow solutions; one solution covers the odd grid-levels, while the other spans the even levels.

The next section describes use of a template mesh to help plan and define the block topology of the multi-block grid system.

IV. Template Grid

In order to gain a better understanding of how the topology of the WB grid should be laid out, several coarse template grids were studied. These template grids were generated using the globally-elliptic meshing (GEM) method of Vassberg.^{11,12} In short, GEM is based on Green's function; the geometry surface is electrically charged to a constant potential ($\phi = 1$) and the surface grid is extruded along field lines through monotonically-decreasing iso-potential surfaces towards the farfield ($\phi \rightarrow 0$). Based on these dry runs, as well as considering limitations on grid sizes supported by unformatted plot3d files, the surface geometry is partitioned into the blocks depicted in Figure 4. The resolution of the surface grid in this figure is comparable

to the $L = 1$ grid level (designated *Tiny*) of the present unified multi-block grid system. Figure 5 provides the $\phi = 1$ iso-surface, corresponding to the CRM WB geometry. Figures 5-8 illustrate how the surface grid is extruded towards the farfield through iso-potential surfaces of $\phi = [1.000, 0.837, 0.543, 0.222]$, respectively.

The next section details grid dimensions and other pertinent characteristics of the unified baseline multi-block grid.

V. Multi-Block Grid Family

Characteristics of the unified baseline multi-block grid system are included in this section. In general, the layout of the final grid is equivalent to that of the template grid discussed above and depicted in Figures 5-8. Some details of the surface grid of Figure 5, however, have been improved.

Table I provides an overview of the grid family, which is comprised of 6 meshes. In increasing size order, the members of this family are named: *Tiny*, *Coarse*, *Medium*, *Fine*, *ExtraFine* & *SuperFine*, and labeled $[T, C, M, F, X, S]$, respectively. Note that the grids range in size from $\sim 640K$ to $\sim 138M$ hexahedral cells. Recall that the Medium mesh is representative of current practices for accurate drag predictions. In order to accurately capture the viscous shear-stresses in the boundary layer of the Medium mesh, the normal spacing of the first cell next to the wall is $\Delta_1 = 1.0Y^+$. Further, the first 4 cells next to the wall are constantly spaced. These values of Δ_1 and $\#\Delta_1s$ for the other grid-levels are determined by the 2-to-3-to-4 grid refinement. It is anticipated that the asymptotic range of grid convergence will be captured by the $[M, F, X, S]$ meshes.

Table I: Multi-Block Grid Family.

Level	Name	Label	Hexahedra	$\Delta_1 Y^+$	$\# \Delta_1 s$
1	Tiny	T	638,976	2.00	2
2	Coarse	C	2,156,544	1.33	3
3	Medium	M	5,111,808	1.00	4
4	Fine	F	17,252,352	0.67	6
5	ExtraFine	X	40,894,464	0.50	8
6	SuperFine	S	138,018,816	0.33	12

Table II documents additional details of the baseline multi-block grid family. Due to the particular grid-topology adopted, note that the K-dimension (KD) is constant across blocks. Here, $K = 1$ represents the geometry surface, and $K = KD$ is the farfield boundary. A brief walk-around description of each block is included below.

Table II: Block Dimensions.

		Block-1		Block-2		Block-3		Block-4		Block-5		Multigrid
		Fuse-Nose		Fuse-Mid		Wing-IB		Wing-OB		Fuse-Aft		Levels
L	KD	ID	JD	ID	JD	ID	JD	ID	JD	ID	JD	M
1	49	33	33	129	33	129	17	129	33	33	65	5
2	73	49	49	193	49	193	25	193	49	49	97	4
3	97	65	65	257	65	257	33	257	65	65	129	6
4	145	97	97	385	97	385	49	385	97	97	193	5
5	193	129	129	513	129	513	65	513	129	129	257	7
6	289	193	193	769	193	769	97	769	193	193	385	6

Block 1 abuts the surface of the fuselage-nose region. $I = 1$ defines the symmetry plane that abuts the fuselage keel-line. $I = ID$ is the symmetry plane at the fuselage crown-line. $J = 1$ defines the symmetry plane forward of the fuselage nose. $J = JD$ is an interior boundary that abuts blocks 2, 3 and 4.

Block 2 is adjacent to the mid-section of the fuselage barrel. The I-direction is periodic; it wraps around the wing, from the lower TE wake across the lower fuselage to the LE then over the upper fuselage back to the TE wake. Both $I = 1$ and $I = ID$ define the branch-cut at the wing wake, and are identical surfaces. $J = 1$ is comprised of portions that reside on the symmetry plane at the fuselage keel- and crown-lines,

and include portions that are interior boundaries that interface with blocks 1 and 5. $J = JD$ is an interior boundary at the wing-body intersection that abuts block 3.

Blocks 3 and 4 cover the wing, inboard and outboard of the planform break, respectively. Their I and J orientations are equivalent to those of block 2. Again, $I = 1$ and $I = ID$ are identical surfaces at the branch-cut of the wing wake. $J = 1$ and $J = JD$ are interior block interfaces. However, the $J = JD$ computational plane of block 4 is a self-abutting surface that folds over on itself at the LE I -index.

Block 5 covers the aft-fuselage geometry. $I = 1$ defines the symmetry plane that abuts the fuselage keel-line. $I = ID$ is the symmetry plane at the fuselage crown-line. $J = 1$ is an interior boundary that abuts blocks 2, 3 and 4. $J = JD$ defines the symmetry plane behind the fuselage tail-cone.

This concludes our discussion on the unified baseline multi-block grid in preparation for DPW-V. However, in closing, we note that this grid will be translated to other formats such as over-set and unstructured-mesh grids. The various unstructured-mesh types will include: 1) purely hexahedral cells, 2) purely tetrahedral elements, and 3) hybrid with tetrahedra, pyramids, and prisms.

VI. Summary

A unified baseline grid family is presented. This grid system is currently under development for the Fifth AIAA CFD Drag Prediction Workshop. Foundation of the unified system is a family of point-matched multi-block grids. This sequence of grids is built from an *extra-fine* multi-block mesh about the NASA Common Research Model Wing-Body configuration. A *super-fine* mesh is then created by increasing the number of cells in each computational direction by a factor of 1.5, while maintaining grid distribution. The ratio of hexahedral cells between the extra-fine and super-fine meshes is $3.375 = 1.5^3$. These two mesh systems correspond to grid levels 5 & 6, respectively, of the multi-block grid family. To complete the even set of grid levels [2, 4, 6], the super-fine grid is recursively coarsened, consistent with the multigrid technique. In a similar manner, the odd set, comprised of grid levels [1, 3, 5], is constructed beginning with the extra-fine grid. These two groups are then interleaved to yield the final multi-block family of 6 self-consistent grids. Sizes of these grids range from 638, 976 hexahedra of the *tiny* grid system, to 138, 018, 816 cells of the *super-fine* level, a grid-size-ratio of 216. The foundational multi-block grid family will then be converted to other grid types, such as over-set grids and unstructured meshes. Unstructured-grid systems will include families comprised of: 1) all tetrahedral elements, 2) all hexahedral cells, and 3) mixed tetrahedra, prisms, and pyramids.

References

- ¹D. W. Levy, J. C. Vassberg, R. A. Wahls, T. Zickuhr, S. Agrawal, S. Pirzadeh, and M. J. Hemsch. Summary of data from the first AIAA CFD Drag Prediction Workshop. *AIAA Journal of Aircraft*, 40(5):875–882, Sep–Oct 2003.
- ²M. J. Hemsch. Statistical analysis of CFD solutions from the Drag Prediction Workshop. *AIAA paper 2002-0842*, 40th AIAA Aerospace Sciences Meeting & Exhibit, Reno, NV, January 2002.
- ³K. R. Laffin, J. C. Vassberg, R. A. Wahls, J. H. Morrison, O. Brodersen, M. Rakowitz, E. N. Tinoco, and J. Godard. Summary of data from the second AIAA CFD Drag Prediction Workshop. *AIAA Journal of Aircraft*, 42(5):1165–1178, 2005.
- ⁴M. Hemsch and J. Morrison. Statistical analysis of CFD solutions from 2nd Drag Prediction Workshop. *AIAA Paper 2004-0556*, 42nd AIAA Aerospace Sciences Meeting and Exhibit, Reno, NV, January 2004.
- ⁵J. C. Vassberg, E. N. Tinoco, M. Mani, O. P. Brodersen, B. Eisfeld, R. A. Wahls, J. H. Morrison, T. Zickuhr, K. R. Laffin, and D. J. Mavriplis. Abridged summary of the third AIAA CFD Drag Prediction Workshop. *AIAA Journal of Aircraft*, 45(3):781–798, May–June 2008.
- ⁶J. H. Morrison and M. J. Hemsch. Statistical analysis of CFD solutions from the third AIAA Drag Prediction Workshop. *AIAA Paper 2007-0254*, 45th AIAA Aerospace Sciences Meeting and Exhibit, Reno, NV, January 2007.
- ⁷J. C. Vassberg, E. N. Tinoco, M. Mani, T. Zickuhr, D. W. Levy, O. P. Brodersen, B. Eisfeld, R. A. Wahls, J. H. Morrison, D. J. Mavriplis, and M. Murayama. Summary of the Fourth AIAA CFD Drag Prediction Workshop. *AIAA Paper 2010-4547*, 28th AIAA Applied Aerodynamics Conference, Chicago, IL, June 2010.
- ⁸J. H. Morrison. Statistical analysis of CFD solutions from the Fourth AIAA Drag Prediction Workshop. *AIAA Paper 2010-4673*, 28th AIAA Applied Aerodynamics Conference, Chicago, IL, June 2010.
- ⁹4th AIAA CFD Drag Prediction Workshop. <http://aaac.larc.nasa.gov/tsab/cfdlarc/aiaa-dpw/>, dpw@cessna.textron.com, San Antonio, TX, June 2009.
- ¹⁰J. C. Vassberg, M. A. DeHaan, S. M. Rivers, and R. A. Wahls. Development of a Common Research Model for applied CFD validation studies. *AIAA Paper 2008-6919*, 26th AIAA Applied Aerodynamics Conference, Hawaii, HI, August 2008.
- ¹¹J. C. Vassberg. Multi-block mesh extrusion driven by a globally elliptic system. *Conference Proceedings*, 5th U.S. National Congress on Computational Mechanics, 2nd Symposium on Trends in Unstructured Mesh Generation, Boulder, CO, August 1999.
- ¹²J. C. Vassberg. Further study of globally elliptic meshing. *Conference Proceedings*, 7th International Conference on Numerical Grid Generation in Computational Field Simulations, Whistler, British Columbia, Canada, September 2000.

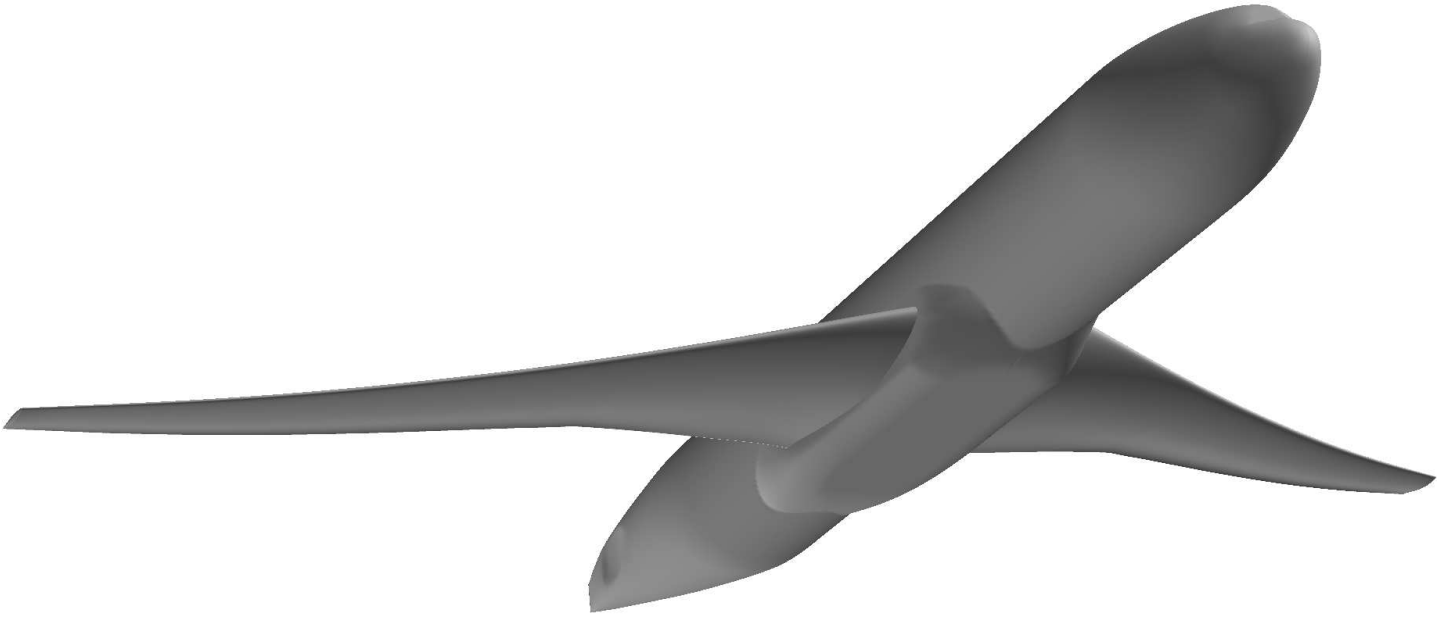


Figure 1. NASA CRM Wing-Body Configuration, Lower-Front View.

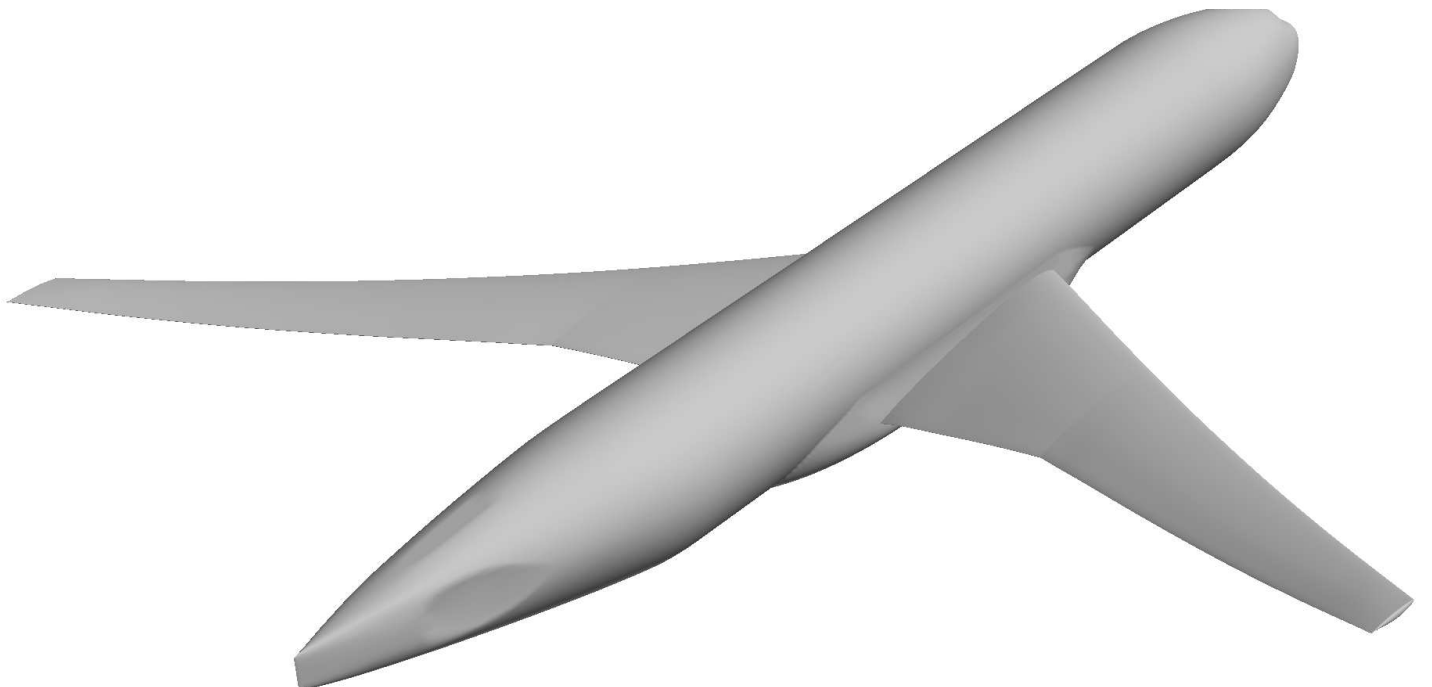


Figure 2. NASA CRM Wing-Body Configuration, Upper-Aft View.

Grid-Spacing Trends of Grid Families

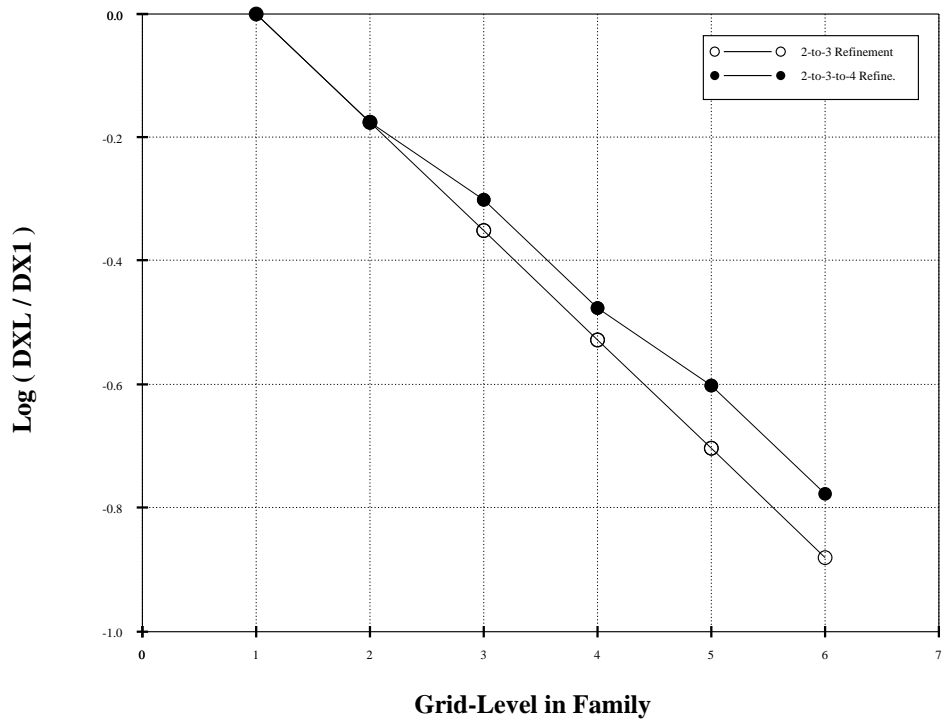


Figure 3. Cell-Size Trends in Grid Families.

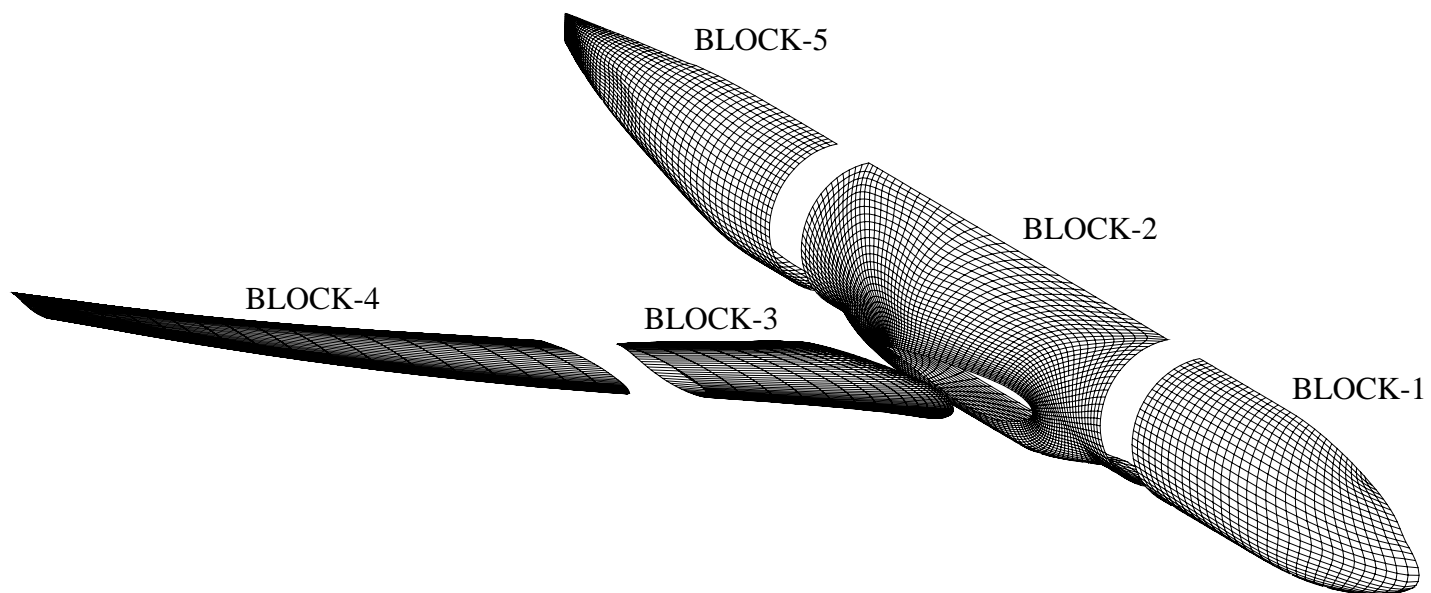


Figure 4. Block Topology for the CRM Wing-Body Multi-Block Grid Family.

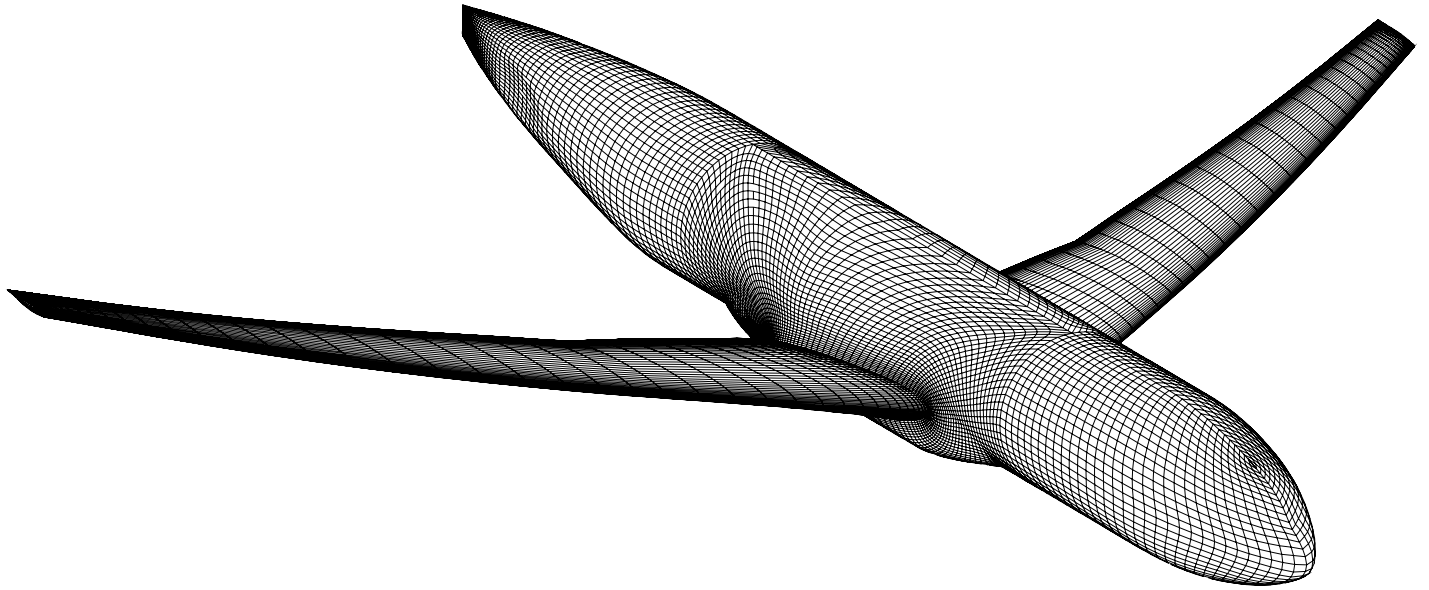


Figure 5. Template Grid $\phi = 1.000$ Iso-Surface.

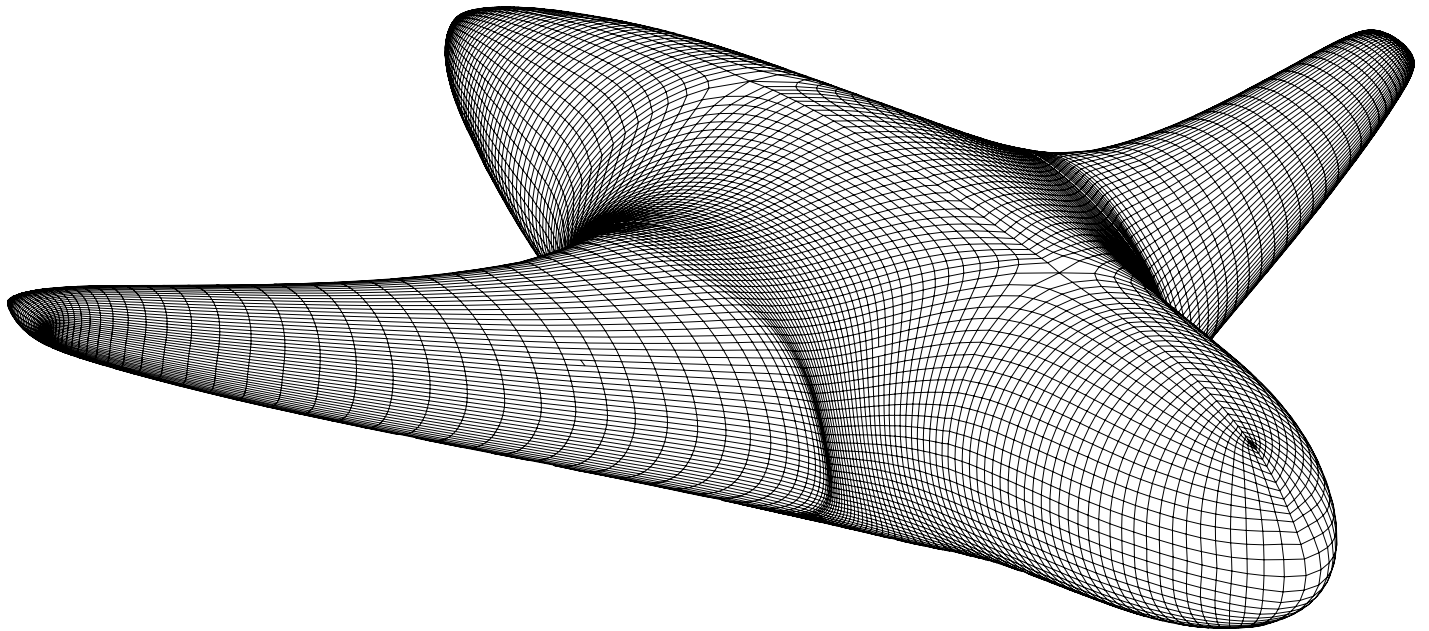


Figure 6. Template Grid $\phi = 0.837$ Iso-Surface.

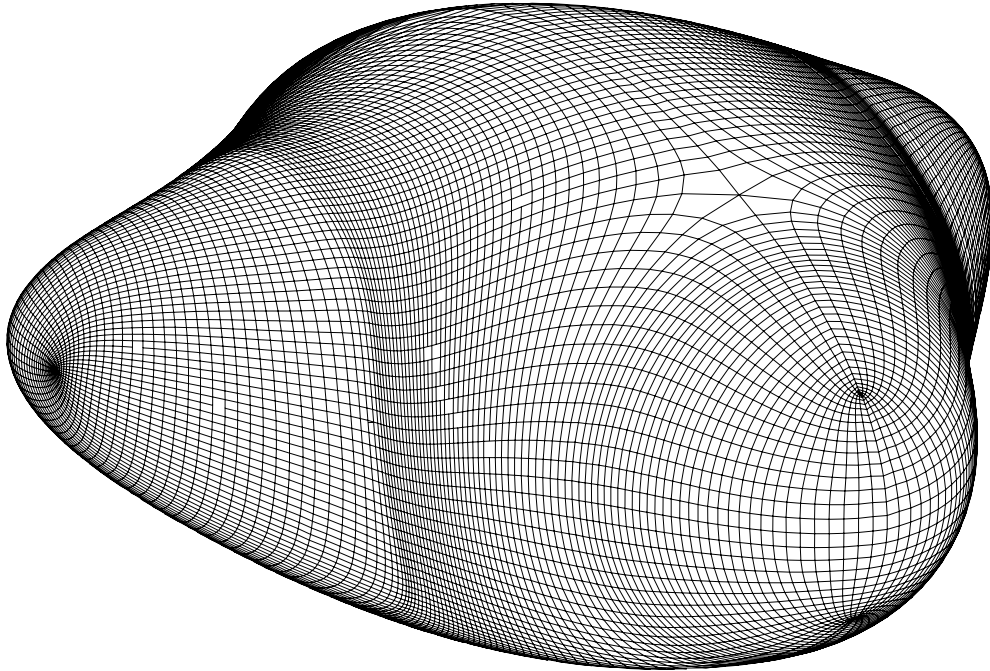


Figure 7. Template Grid $\phi = 0.543$ Iso-Surface.

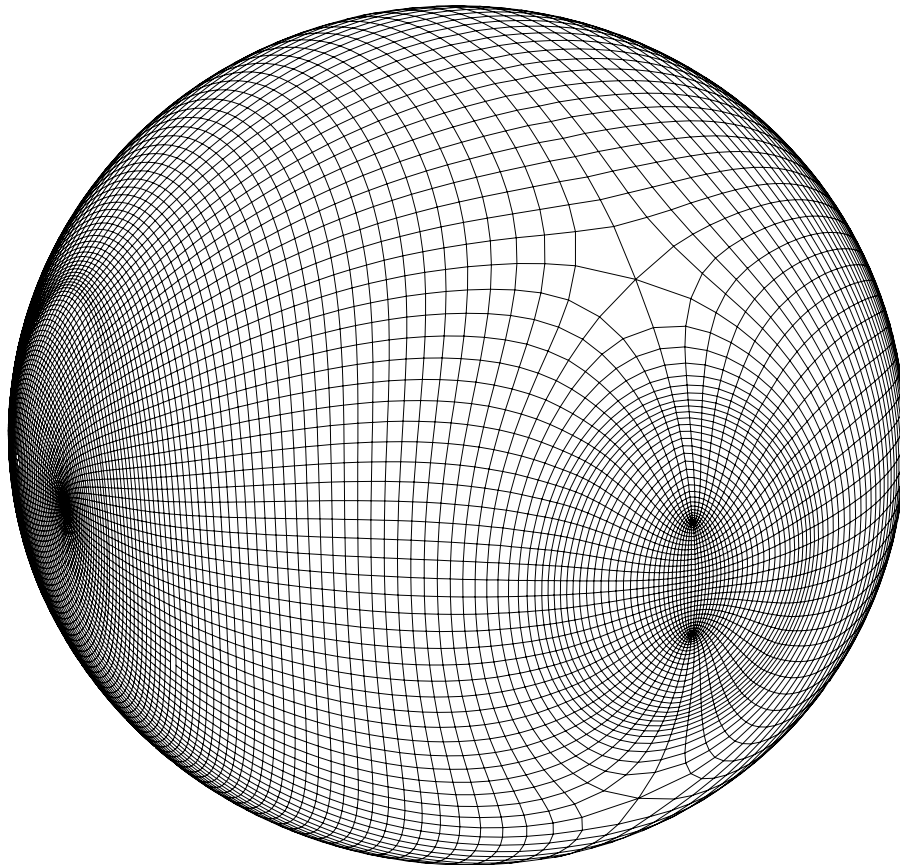


Figure 8. Template Grid $\phi = 0.222$ Iso-Surface.